# A Bidirectional Deep Neural Network for Accurate Silicon Color Design

*Li Gao,\* Xiaozhong Li, Dianjing Liu, Lianhui Wang, and Zongfu Yu\**

Silicon nanostructure color has achieved unprecedented high printing resolution and larger color gamut than sRGB. The exact color is determined by localized magnetic and electric dipole resonance of nanostructures, which are sensitive to their geometric changes. Usually, the design of specific colors and iterative optimization of geometric parameters are computationally costly, and obtaining millions of different structural colors is challenging. Here, a deep neural network is trained, which can accurately predict the color generated by random silicon nanostructures in the forward modeling process and solve the nonuniqueness problem in the inverse design process that can accurately output the device geometries for at least one million different colors. The key results suggest deep learning is a powerful tool to minimize the computation cost and maximize the design efficiency for nanophotonics, which can guide silicon color manufacturing with high accuracy.

Structural colors generated by metallic plasmonic resonance such as gold, aluminum, and magnesium possess an ultra-high resolution of ≈100 000 dots per inch, which is superior to regular printing technologies and shows great potential in passive color display and information storage applications.[1–3] However, metallic nanoplasmonic structures show poor color saturation and limited coverage on International Commission on Illumination (CIE) 1931 chromaticity diagram, which are not ideal for vivid, high-quality colored display.[4] Fortunately, this issue has been tackled by recently reported plasmonic color filters having dual resonance modes with proper orthogonality[5] or silicon nanostructure with an index matching layer

that satisfies Kerker's condition.[6] The latter generated colors are highly saturated and occupy the largest color gamut to date on the CIE chromaticity diagram, with additional benefits of viewing-angle independence and complementary metal-oxide-semiconductor process compatibility. Therefore, silicon colors hold promise in realistic display, imaging, and data storage applications.

Current structural color design follows the conventional design strategy, which heavily relies on full electromagnetic (EM) simulation. The exact resonance spectrum and desired properties are simulated and optimized by tuning characteristic device geometries. Such an approach has been successful in obtaining small-scale, simple resonant structures for the past years. However, as the complexity and device scale increases, it becomes challenging to optimize multiple parameters simultaneously, which usually takes days or weeks to perform a large number of parameter sweeps. Such computational cost is high since only the optimized results are useful, while all other simulation data become useless and wasted. In addition, the previous structural color design has only realized a few hundreds of silicon nanostructures that show distinctive color,[6] which is far less satisfying for real applications where advanced displays consist of millions of different colors. Conventional EM simulation can hardly produce such an enormous amount of data efficiently.

Artificial neural networks (ANNs) can emulate the biological, structural, and functional features of biological neural networks.[7] The application of ANNs has emerged recently showing power new capabilities in various scenario including computer vision, speech and face recognition, language and image processing, etc. A deep learning approach can analyze the scattering spectra of silicon nanostructure within the diffraction-limited area and output digital information, which breaks the limits of optical information storage and already beats the Blu-ray Disk technology.[8] In the field of nanophotonics, computational inverse design can reshape the landscape and techniques available to complex and emerging applications.[9] Recent advancements in deep neural networks (DNNs) have demonstrated efficient forward-modeling that can predict resonance spectrum accurately, and perform the inverse design of photonic device structures.[10–18] The general steps usually involve a one-time investment of sufficient EM simulation data, which are composed of variable device parameters and corresponding optical resonance at different wavelengths, followed by constructing DNNs. In a forward modeling network,

Prof. L. Gao, Prof. L. Wang
Key Laboratory for Organic Electronics and Information Displays (KLOEID)
Institute of Advanced Materials (IAM)
School of Materials Science and Engineering
Nanjing University of Posts and Telecommunications
Nanjing 210023, China
E-mail: iamlgao@njupt.edu.cn
X. Li
School of Electronic and Optical Engineering
Nanjing University of Science and Technology
Nanjing 210094, China
D. Liu, Prof. Z. Yu
School of Electrical and Computer Engineering
University of Wisconsin-Madison
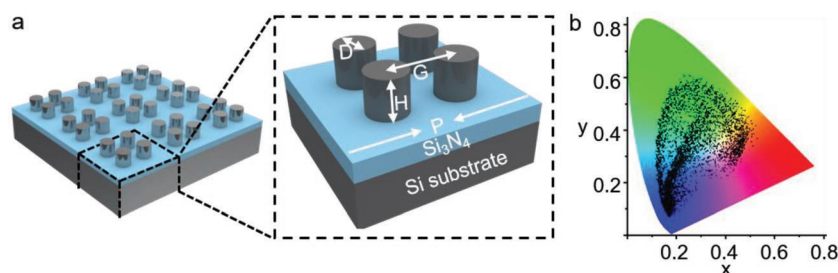Madison, WI 53706, USA
E-mail: zyu54@wisc.edu

1905467 (1 of 7)

**Figure 1.** Schematic illustration of the silicon nanostructure and the generated colors. a) The studied geometry parameters include the diameter (*D*) and height (*H*) of nanodisks, the gap (*G*) between nanodisks in a unit and the period (*P*) of repeating units. b) The coverage of training data generated colors on the CIE 1931 chromatic diagram.

the input takes the structural parameters and the network outputs optical properties such as spectra. An iterative process can be used to optimize the input structural parameters to accomplish the goal of the inverse design.[14] In contrast, in an inverse design network,[11] the desired optical properties are taken as the input, and the network directly outputs the device structures. This method eliminates the iterative optimization process.

Here, we develop an inverse design DNN as a practical and accurate design tool for generating a large amount of silicon structural colors. We used a relatively small amount of full-wave EM simulations as the training data. First, a forward DNN is trained to directly connect device geometry to color values. Then, we used a tandem network architecture[11] to effectively overcome the nonuniqueness problem encountered in the inverse design process. The results include a highly accurate forward tool to predict color values from silicon structures, and an inverse design tool that maps color to structures. It covers over a million of ultra-dense color points on the CIE chromaticity diagram which has not been achieved previously.

In this work, our illustration applied a similar silicon nanostructure with an index matching layer of 70 nm $Si_3N_4$ on silicon substrate as reported before.[6] Such condition can mimic

Si nanostructure in free space and satisfy Kerker's condition for distinctive sharper optical resonances. We focus on a unit cell that has four equally spaced and shaped nanodisks as shown in **Figure 1**a. The most critical factors here affecting the optical resonances are the diameter (*D*) and height (*H*) of individual nanodisk, the gap (*G*) between neighboring nanodisks in a unit cell, and the period (*P*) of repeating unit cells. The diameter ranges from 80 to 160 nm, the height from 30 to 200 nm, the center-to-center gap from 160 to 320 nm, and the unit period from 300 to 700 nm. It allows us to reach a broader range of color than the previous study.[5,6] We use the finite-different time-domain method to simulate 4660 samples with different parameter combinations. The reflectance spectra are obtained from 380 to 780 nm. By converting all the reflectance spectra into *x*, *y*, *Y* values through color matching functions as discussed in Section S1 in the Supporting Information, we completed the training data collection. All the obtained colors are plotted in the CIE chromaticity diagram shown in Figure 1b. The color space achievable by studied silicon nanostructures is ranged from 0.11 to 0.53 for *x*, 0.08 to 0.62 for *y*, and 0.01 to 0.64 for *Y*, they are estimated to occupy an area that is 143% of sRGB color space (Section S2, Supporting Information), which is about 23% larger compared to previous study.[5,6]

The influence of different Si geometric parameters on the reflectance spectrum and colors is displayed in **Figure 2**a–d and Section S3 in the Supporting Information. Changes in the geometric parameters can result in shifts in the resonance peaks and features that are well understood by EM theories. The color values (*x*, *y*, *Y*) calculated from the reflectance spectrum are thus different and display different colors. As shown in the graphs, by keeping all other three parameters fixed, changes in a single parameter can induce resonance feature changes. When the period of repeating unit cell changes from 400 to
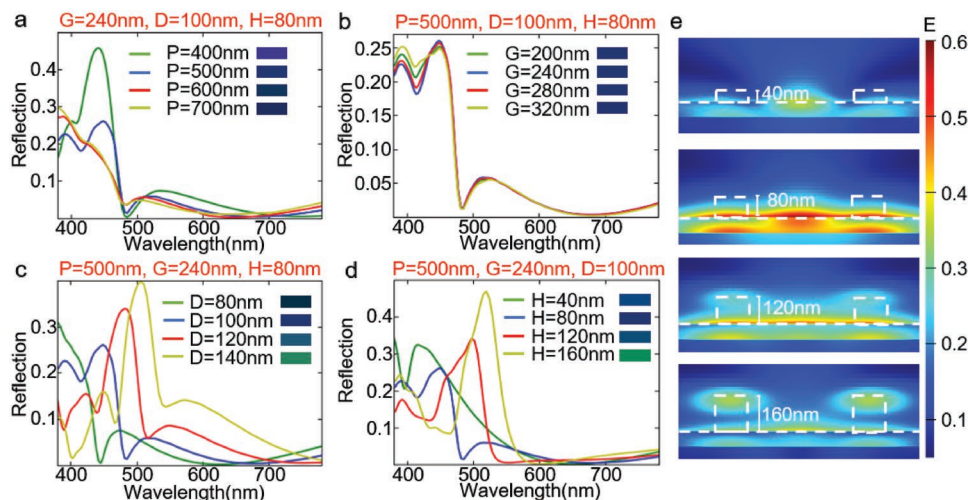


**Figure 2.** Four studied silicon nanostructure geometric parameters that affect the reflectance spectrum. a–d) The reflectance spectrum changes with period (a), gap (b), diameter (c), and height (d) while fixing the other three parameters. e) The electric field intensity change with different heights shown in (d).

700 nm, the reflectance spectrum and corresponding color images are plotted in Figure 2a. The calculated maximum color changes are $\Delta x = 0.0217$, $\Delta y = 0.0116$, $\Delta Y = 0.0321$. In the case of gap changes from 200 to 320 nm, the reflectance spectrum shows little feature changes, and we can hardly observe the color changes by human eyes as shown in Figure 2b, the color values change only by $\Delta x = 0.0012$, $\Delta y = 0.0001$, $\Delta Y = 0.0005$. Diameter and height play a bigger role in tuning the reflectance spectrum, as seen in Figure 2c, by increasing diameter from 80 to 140 nm, the reflectance peak can shift to longer wavelengths, thus resulting in less blue colors, the exact changes in color values are $\Delta x = 0.1010$, $\Delta y = 0.1850$, $\Delta Y = 0.1552$. Increases in the height of the nanodisks in Figure 2d show similar trends that thinner nanodisks are bluer with the color value changes of $\Delta x = 0.0244$, $\Delta y = 0.3073$, $\Delta Y = 0.1016$. The electric field intensity simulated for different nanodisk heights is displayed in Figure 2e, which shows completely different electric dipole resonance properties. To further test the color sensitivity to geometry changes in height, by fixing $P = 500$ nm, $G = 240$ nm, $D = 100$ nm, the slight change of $H$ from 120 to 121 nm can result in an observable change of $\Delta x = 0.0015$, $\Delta y = 0.0078$, $\Delta Y = 0.0023$. If we take all four parameter changes into account, the complexity will increase drastically and the total number of possible combinations can be as big as $8.7 \times 10^8$ at a step size of 1 nm. It becomes very difficult to simulate this huge amount of data and obtain all generated color values through conventional computation methods.

Deep learning approach by DNNs can address such a challenge in computation and design. We start with a forward modeling network for accurate and instant prediction of colors that are generated by silicon nanostructures. Unlike many previous NN studies of nanophotonics that use geometric parameters as the input layer and spectrum as the output layer, we eliminate spectrum data in our network and directly construct a fully connected network between silicon nanostructure parameters ($D$, $H$, $G$, $P$) to color values ($x$, $y$, $Y$) as seen in **Figure 3**a. In the training process, datasets are split into three parts: training data, validation data, and test data. Training data are fed to the NN to optimize the network by updating weights; validation data are used to examine the network, serving as a check of the trained effect and helping us learn that whether the network is overfitting; test data use completely new data to test the accuracy of the prediction. Our study used 3900 groups of EM simulation data for network training, 400 groups of data for network validation, and 360 groups of data for result testing. The fundamental DNNs hyperparameter choices are referred to previous studies[14] and shown in Section S4, Table S1 in the Supporting Information. The optimum network architecture is determined to have four hidden layers with 320 nodes in each layer. During the deep learning process, the NN continuously adjusts each connection weights with every batch of data in epochs, and validation data were fed to the network every ten epochs to evaluate the effect of NN, with an optimized batch size of 10. As there is always a unique response for every parameter combination, the training is easy to converge. The validation error over epochs is plotted in Figure 3b and it drops continuously as the training goes on. The validation mean square error becomes $1.03 \times 10^{-5}$ after 900 epoch of training, after which the cost function of this learning curve barely drops and the training is complete. Comparison with other tested network architectures is tabled in
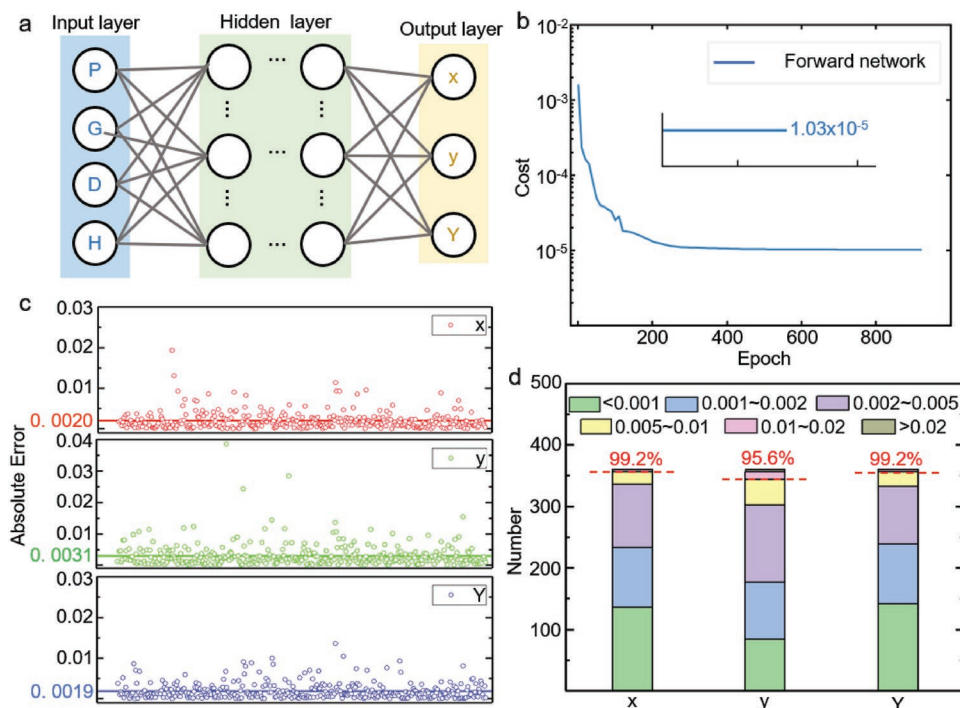


**Figure 3.** The forward modeling neural network for predicting Si structural colors. a) DNNs architecture with input layer of geometric parameters $P$, $G$, $D$, and $H$, hidden layers and output layer of color values $x$, $y$, and $Y$. b) The cost function of validation errors in the network training process. c) The absolute error of testing results, the top, middle, and bottom panels are the differences in $x$, $y$, and $Y$ between predicted color values and true color values. d) Statistics of the testing results where majority of color values shows discrepancy below 0.01.

Section S4, Table S2 in the Supporting Information. To test the accuracy of this NN, we use 360 groups of EM simulation data that the network has not been trained on. We compare the color values predicted by the DNNs and those obtained by EM simulations. The results are plotted in Figure 3c. The top, middle, and bottom panels are the absolute differences in $x$, $y$, and $Y$ values. The average discrepancies are 0.0020, 0.0031, 0.0019, respectively, which proves the prediction is highly accurate. By statistical analysis shown in Figure 3d, over 99% prediction has a difference less than 0.01 for $x$ and $Y$, and over 95% for that of $y$. Since $x$, $y$, $Y$ all have values from 0 to 1, this network can output approximately 100 different values for each of $x$, $y$, $Y$ with over 95% confidence, which means one million different color capacity on the CIE chromaticity diagram.

On the other hand, for broader interests in lithography-oriented structural color design and fabrication research, we still lack a common tool to realize the inverse design of precisely structured devices. Usually, we want a specific structural color and need to know the corresponding device structure such as $P$, $G$, $D$, and $H$ that can be produced by advanced lithographic tools. If we can input known values of $x$, $y$, $Y$ and output the device geometric parameters directly, it will greatly reduce the design optimization time and help prototype new device colors quickly. To realize this purpose, we first set up a simple, inverse DNNs by using color values in the input layer and device parameters in the output layer. However, the training is not successful which can be seen from Table S3 in the Supporting Information with large losses. The reason is due to a severe nonuniqueness problem since many combinations of different device geometric parameters can generate similar color values and the network can hardly converge in the inverse direction. There are two scenarios; the first case is that different nanostructures can produce similar spectrum which exhibits similar colors; this can be partly inferred from Figure 2b plots. The second case happens when different nanostructures do produce different spectra, but through color matching function, the colors produced can also be very similar to each other. Let us take one example to illustrate either case, for the parameters of $P = 450$ nm, $G = 250$ nm, $D = 110$ nm, and $H = 150$ nm, the color generated is $x = 0.1954$, $y = 0.5554$, and $Y = 0.3071$ while for parameters of $P = 470$ nm, $G = 220$ nm, $D = 131$ nm, and $H = 107$ nm, the color generated is $x = 0.1973$, $y = 0.5545$, and $Y = 0.3086$. These color values are very similar to each other, thus their solutions of corresponding geometric parameters can be nonunique. When there are one to many solutions, in the inverse DNNs training, the weights applied to one of the solutions may be then changed by another one in the training afterward, which make the training difficult to converge. In order to solve this problem, we adopt the tandem network as shown in **Figure 4**a. Here, we connect the inverse network to the pretrained forward network which has already been trained independently. The forward network takes the geometric parameters ($P$, $G$, $D$, $T$) as input and outputs color values ($x$, $y$, $Y$). In the tandem network, desired color values ($x$, $y$, $Y$) are taken as the input. The output is the designed structure ($P$, $G$, $D$, $T$) denoted as the intermediate layer. The output of the pretrained forward network is the color values ($x'$, $y'$, $Y'$) calculated from the designed structure. The weights in the pretrained forward
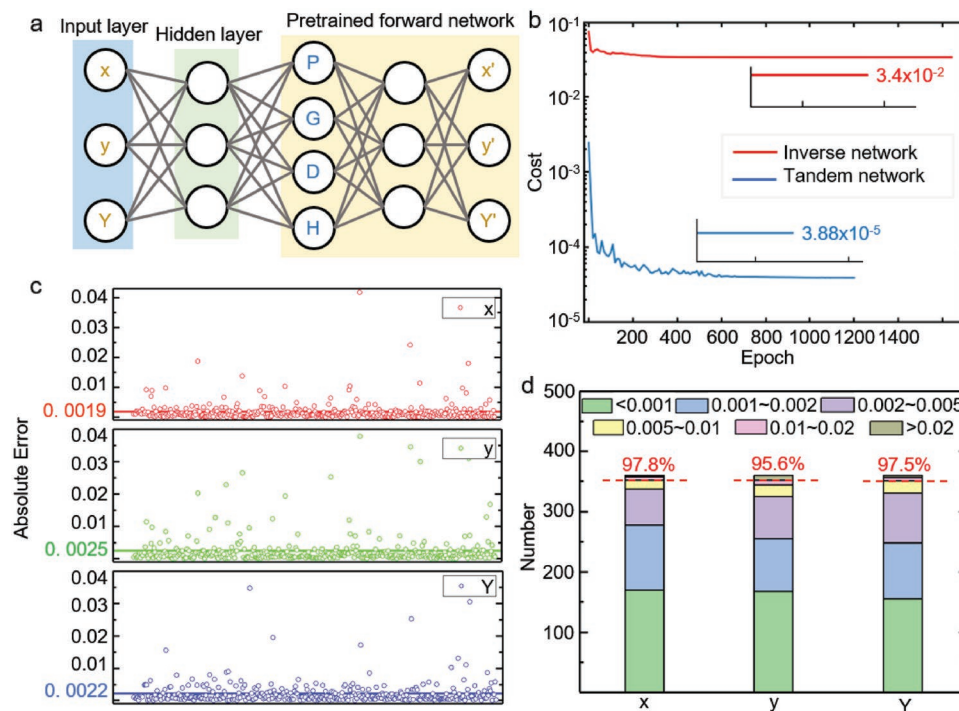


**Figure 4.** The inverse design neural network for predicting Si structural colors. a) Tandem DNNs architecture with input layer of color values $x$, $y$, and $Y$, hidden layers, and connected pretrained forward modeling network. b) The cost function of validation errors in the network training process of a direct inverse network and a tandem network. c) The absolute error of testing results, the top, middle, and bottom panels are the differences in $x$, $y$, and $Y$ between inverse-designed color values and desired color values. d) Statistics of the testing results where majority of color values shows discrepancy below 0.01.

ADVANCED
SCIENCE NEWS
www.advancedsciencenews.com

ADVANCED
MATERIALS
www.advmat.de

modeling network are fixed and the weights in the tandem network are trained to reduce the cost function defined as the error between the output designed color values ($x'$, $y'$, $Y'$) and the input desired color values ($x$, $y$, $Y$). As seen in Figure 4b, the validation error decreases rapidly for tandem network and reaches $3.88 \times 10^{-5}$ which is significantly lower than a simple inverse network that has a huge training loss of $3.4 \times 10^{-2}$. This tandem network structure thus overcomes the issue of nonuniqueness between color and structure. The best inverse network architecture is determined to have four layers with each layer having 300 nodes as discussed in Table S4 in the Supporting Information. We again use 360 groups of data to test the accuracy of inverse design process, the desired color values ($x$, $y$, $Y$) are input into the network to output the designed color values ($x'$, $y'$, $Y'$), and find out the average deviation from the true values are 0.0019, 0.0025, and 0.0022 (Figure 4c). Statistically as shown in Figure 4d, over 95% of $x$, $y$, and $Y$ values have errors below 0.01 which means we can also inverse design one million different colors with over 95% accuracy. A recent study by deep learning method has been reported for a specific case of plasmonic color induced by laser ablation and deposition.[19] The geometric parameters of the average particle diameter, spacing and embedding depth, and the correlated laser parameters can be predicted from color information using an iterative multivariable inverse design method. The mean percent error

of inverse-designed RGB color values is around 5%, leading to a color difference that is still observable by human eyes. This work shows significantly higher accuracy that the difference in colors can hardly be perceived.

We take a specific example to illustrate the DNNs application process and show its convenience and accuracy. The conventional design process is displayed in **Figure 5**a, which starts with a set of geometric parameters by intuition and experiences, such as $P = 500$ nm, $G = 300$ nm, $D = 150$ nm, $H = 65$ nm, we then obtain the reflectance spectrum, followed by using the color matching function to convert the spectrum into color values that we can observe on the CIE chromaticity diagram. If the color does not meet the application requirement, this process will be performed iteratively. Figure 5b shows our forward modeling network, here we input the geometric parameters of $P = 500$ nm, $G = 300$ nm, $D = 150$ nm, $H = 65$ nm. We do not need to wait for hours for EM simulations. The network will output the color values ($x$, $y$, $Y$) instantly. The predicted color values agree with those from full-wave simulation very well. Figure 5c shows the inverse design process. We start with desired color values of $x = 0.2978$, $y = 0.4193$, $Y = 0.2250$, and by inputting these values into the tandem network, we can output the designed geometric parameters $P = 473$ nm, $G = 256$ nm, $D = 157$ nm, and $H = 79$ nm. We should note here that this designed structure is very different
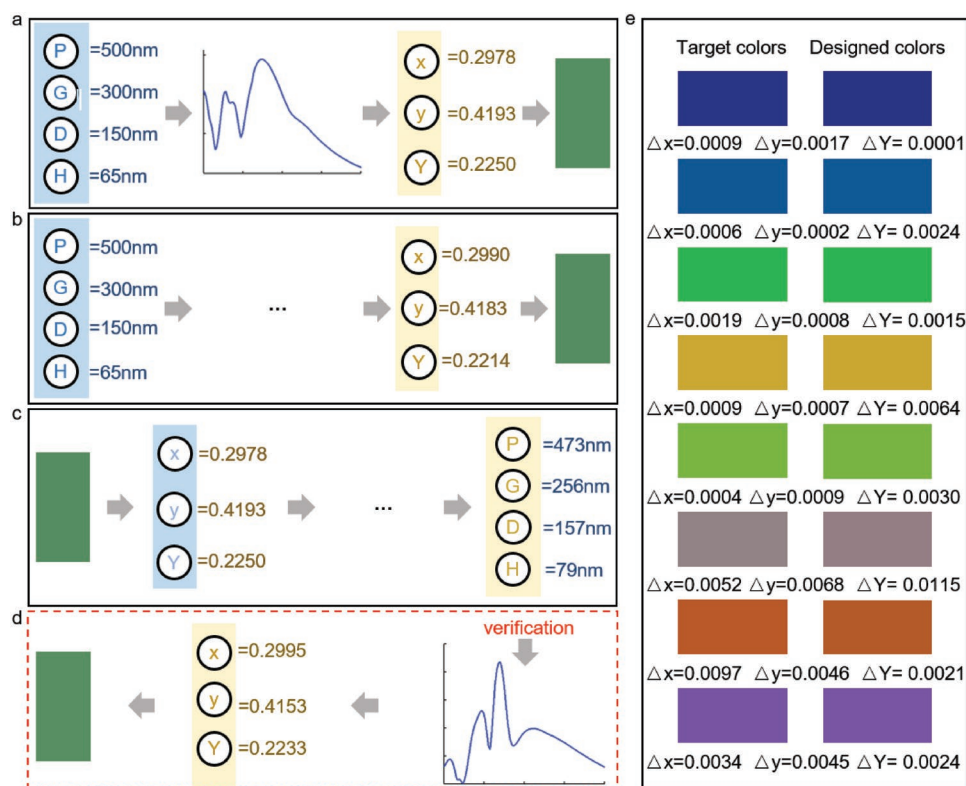


**Figure 5.** The comparison of application process of conventional simulation, forward NN, and inverse design NN. a) The iterative optimization process to obtain desired structural colors. b) The instant output of structural colors by forward modeling network without any EM simulations. c) The inverse design process where desired color values are input in the NN and output the geometric parameters. d) The optional verification of design accuracy, that the inverse design obtained geometric parameters from (c) is simulated to obtain the reflectance spectrum and convert to the color values, the resulted color image is compared to the original desired image. e) Eight groups of desired target colors are inverse designed to obtain corresponding geometric parameters, which generate the designed colors for comparison.
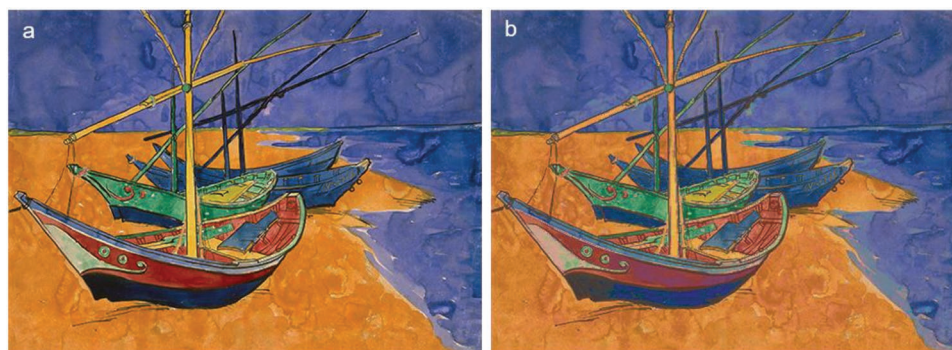
**ADVANCED
SCIENCE NEWS**

www.advancedsciencenews.com

**ADVANCED
MATERIALS**

www.advmat.de

**Figure 6.** The actual application of the DNNs-based structural color design. a) The desired colors of the painting Fishing Boats on the Beach at Saintes-Maries-de-la-Mer by Vincent van Gogh, and b) the inverse-designed structural colors by DNNs. "Fishing Boats on the Beach at Saintes-Maries-de-la-Mer" is reproduced with permission of the Van Gogh Museum, Amsterdam (Vincent van Gogh Foundation).

from the original known structure, which also demonstrates the existence of nonunique solutions for similar colors. Further test is optional but discussed here in Figure 5d to verify the accuracy. Through the conventional simulation process, the color values produced by the designed structure is very close to the desired color values, the absolute differences are only $\Delta x = 0.0017$, $\Delta y = 0.0040$, $\Delta Y = 0.0017$. This illustration proves that the tandem network is a smart and effective tool to obtain a unique and accurate solution for every single color. In Figure 5e, we compare the design results for multiple groups of colors with details displayed in Section S5 in the Supporting Information, the small discrepancies between designed and desired colors show that this inverse design method by tandem DNNs is accurate and repeatable. In the last part, as shown in **Figure 6**a, we extract the color values for all $512 \times 372$ color pixels on the painting of "Fishing Boats on the Beach at Saintes-Maries-de-la-Mer" by Vincent van Gogh and input them into the tandem network. The results can directly output the designed geometric parameters for all the 190 464 pixels on the painting and the generated painting colors are shown in Figure 6b. We can see that the inverse designed colors by the tandem network are extremely accurate for points lie within the boundaries of realizable color space determined by the training datasets. If the color becomes too dark with extremely small $Y$ values, the prediction is not accurate nor producible by silicon nanostructures. It can be observed that the black color with a $Y$ value smaller than 0.001 shows a huge discrepancy on the generated painting. Therefore, this design tool is best suited for vivid, colorful applications and the generated device parameters can be directly adopted in the lithographic process for actual device fabrication and printing. For realistic applications, prototype of variable device parameters can be completed by electron beam lithography for device area over cm$^2$, the mass production of such device can be completed by low-cost, high-throughput techniques such as nanoimprinting and soft lithography reported earlier.[20–24] By current cutting-edge lithography technique, $\approx 10$ nm structural precision is reproducible in physical devices, which would provide approximately 90 000 different silicon structural colors. With further development in nanofabrication technology up to $\approx 5$ nm precision, over 1 million different structural colors are achievable and compatible with our DNNs design tool.

In this work, we show that deep learning can replace costly full-wave EM simulation to design structural color by Si nanostructures. As a design tool, it accomplishes unprecedented speed, reducing the design time by orders of magnitude. By performing a few thousand groups of full EM simulations, it is possible to obtain one million different colors that can cover a large area of CIE chromaticity diagram which is necessary for real display applications. Further studies of various mixed Si nanostructure shapes, sizes, and gaps could expand the color space. Other structural color materials and device systems can also be examined to fully explore larger color space. Moreover, investigation of DNNs that are capable of accurately searching for structures that are outside of current color space would be more challenging and significant. Nonetheless, this deep learning tool provides a general idea for inversely designing multiple parameters in complex nanophotonics and metasurfaces.

## Supporting Information

Supporting Information is available from the Wiley Online Library or from the author.

## Acknowledgements

## Conflict of Interest

The authors declare no conflict of interest.

## Author Contributions

L.G. and X.L. contributed equally to this work. L.G. conceived the project, analyzed the data, and wrote the manuscript. X.L. performed the EM simulations, constructed the NN architecture, and analyzed the data. D.L. and Z.Y. provided the technical guidance and modified the manuscript. L.W. oversaw and supervised this work.

## Keywords

[1] K. Kumar, H. Duan, R. S. Hegde, S. C. W. Koh, J. N. Wei, J. K. W. Yang, *Nat. Nanotechnol.* **2012**, *7*, 557.

[2] S. J. Tan, L. Zhang, D. Zhu, X. M. Goh, Y. M. Wang, K. Kumar, C.-W. Qiu, J. K. W. Yang, *Nano Lett.* **2014**, *14*, 4023.

[3] X. Duan, S. Kamin, N. Liu, *Nat. Commun.* **2017**, *8*, 14606.

[4] A. Kristensen, J. K. W. Yang, S. I. Bozhevolnyi, S. Link, P. Nordlander, N. J. Halas, N. A Mortensen, *Nat. Rev. Mater.* **2017**, *2*, 16088.

[5] H. Kim, M. Kim, T. Chang, A. Baucour, S. Jeon, H. Kim, H.-J. Choi, H. Lee, J. Shin, *Opt. Express* **2018**, *26*, 27403.

[6] Z. Dong, J. Ho, Y. F. Yu, Y. H. Fu, R. Paniagua-Dominguez, S. Wang, A. I. Kuznetsov, J. K. W. Yang, *Nano Lett.* **2017**, *17*, 7620.

[7] Q. Zhang, H. Yu, M. Barbiero, B. Wang, M. Gu, *Light: Sci. Appl.* **2019**, *8*, 42.

[8] P. R. Wiecha, A. Lecestre, N. Mallet, G. Larrieu, *Nat. Nanotechnol.* **2019**, *14*, 237.

[9] S. Molesky, Z. Lin, A. Y. Piggott, W. Jin, J. Vuckovic, A. W. Rodriguez, *Nat. Photonics* **2018**, *12*, 659.

[10] K. Yao, R. Unni, Y. Zheng, *Nanophotonics* **2019**, *8*, 339.

[11] D. Liu, Y. Tan, E. Khoram, Z. Yu, *ACS Photonics* **2018**, *5*, 1365.

[12] W. Ma, F. Cheng, Y. Liu, *ACS Nano* **2018**, *12*, 6326.

[13] Z. Liu, D. Zhu, S. P. Rodrigues, K.-T. Lee, W. Cai, *Nano Lett.* **2018**, *18*, 6570.

[14] J. Peurifoy, Y. Shen, L. Jing, Y. Yang, F. Cano-Renteria, B. G. DeLacy, J. D. Joannopoulos, M. Tegmark, M Soljačič, *Sci. Adv.* **2018**, *4*, eaar4206.

[15] S. Inampudi, H. Mosallaei, *Appl. Phys. Lett.* **2018**, *112*, 241102.

[16] I. Malkiel, M. Mrejen, A. Nagler, U. Arieli, L. Wolf, H Suchowski, *Light: Sci. Appl.* **2018**, *7*, 60.

[17] Y. Chen, J. Zhu, Y. Xie, N. Feng, Q. H. Liu, *Nanoscale* **2019**, *11*, 9749.

[18] E. Bor, O. Alparslan, M. Turduev, Y. S. Hanay, H. Kurt, S. Arakawa, M. Murata, *Opt. Express* **2018**, *26*, 29032.

[19] J. Baxter, A. C. Lesina, J.-M. Guay, A. Weck, P. Berini, L. Ramunno, *Sci. Rep.* **2019**, *9*, 8074.

[20] D. Chanda, K. Shigeta, S. Gupta, T. Cain, A. Carlson, A. Mihi, A. J. Baca, G. R. Bogart, P. Braun, J. A. Rogers, *Nat. Nanotechnol.* **2011**, *6*, 402.

[21] L. Gao, K. Shigeta, A. Vazquez-Guardado, C. J. Progler, G. R. Bogart, J. A. Rogers, D. Chanda, *ACS Nano* **2014**, *8*, 5535.

[22] L. Gao, Y. Kim, A. Vazquez-Guardado, K. Shigeta, S. Hartanto, D. Franklin, C. J. Progler, G. R. Bogart, J. A. Rogers, D. Chanda, *Adv. Opt. Mater.* **2014**, *2*, 256.

[23] L. Gao, Y. Zhang, H. Zhang, S. Doshay, X. Xie, H. Luo, D. Shah, Y. Shi, S. Xu, H. Fang, J. A. Fan, P. Nordlander, Y. Huang, J. A. Rogers, *ACS Nano* **2015**, *9*, 5968.

[24] R. Li, S. Xie, L. Zhang, L. Li, D. Kong, Q. Wang, R. Xin, X. Sheng, L. Yin, C. Yu, Z. Yu, X. Wang, L. Gao, *Nano Res.* **2018**, *11*, 4390.